Systems/Circuits

Behavioral Role of the Reciprocal Inhibition between a Pair of Mauthner Cells during Fast Escapes in Zebrafish

Takashi Shimazaki,[1,2] Masashi Tanimoto,[1] Yoichi Oda,[1] and Shin-ichi Higashijima[2,3]
[1]Division of Biological Science, Graduate School of Science, Nagoya University, Nagoya 464-8602, Japan, [2]National Institutes of Natural Sciences, Exploratory Research Center on Life and Living Systems, National Institute for Basic Biology, Okazaki, Aichi 444-8787, Japan, and [3]Graduate University for Advanced Studies, Okazaki, Aichi 444-8787, Japan

During many behaviors in vertebrates, the CNS generates asymmetric activities between the left and right sides to produce asymmetric body movements. For asymmetrical activations of the CNS, reciprocal inhibition between the left and right sides is believed to play a key role. However, the complexity of the CNS makes it difficult to identify the reciprocal inhibition circuits at the level of individual cells and the contribution of each neuron to the asymmetric activity. Using larval zebrafish, we examined this issue by investigating reciprocal inhibition circuits between a pair of Mauthner (M) cells, giant reticulospinal neurons that trigger fast escapes. Previous studies have shown that a class of excitatory neurons, called cranial relay neurons, is involved in the reciprocal inhibition pathway between the M cells. Using transgenic fish, in which two of the cranial relay neurons (Ta1 and Ta2) expressed GFP, we showed that Ta1 and Ta2 constitute major parts of the pathway. In larvae in which Ta1/Ta2 were laser-ablated, the amplitude of the reciprocal IPSPs dropped to less than one-third. Calcium imaging and electrophysiological recording showed that the occurrence probability of bilateral M-cell activation upon sound/vibration stimuli was greatly increased in the Ta1/Ta2-ablated larvae. Behavioral experiments revealed that the Ta1/Ta2 ablation resulted in shallower body bends during sound/vibration-evoked escapes, which is consistent with the observation that increased occurrence of bilateral M-cell activation impaired escape performance. Our study revealed major components of the reciprocal inhibition circuits in the M cell system and the behavioral importance of the circuits.

Key words: escape; Mauthner cell; reciprocal inhibition; T reticular neuron; zebrafish

Significance Statement

Reciprocal inhibition between the left and right side of the CNS is considered imperative for producing asymmetric movements in animals. It has been difficult, however, to identify the circuits at the individual cell level and their role in behavior. Here, we address this problem by examining the reciprocal inhibition circuits of the hindbrain Mauthner (M) cell system in larval zebrafish. We determined that two paired interneurons play a critical role in the reciprocal inhibition between the paired M cells and that the reciprocal inhibition prevents bilateral firing of the M cells and is thus necessary for the full body bend during M cell-initiated escape. Further, we discussed the cooperation of multiple reciprocal inhibitions working in the hindbrain and spinal cord to ensure high-performance escapes.

Introduction

Vertebrates possess a bilateral CNS consisting of left and right sides of the brain and spinal cord (Holland et al., 2013). Whereas the bilateral CNS works symmetrically in some behaviors (e.g., during hopping or galloping) (Bellardita and Kiehn, 2015; Kiehn, 2016), in many cases it works asymmetrically between the left and right sides, such as when animals swim, walk, run, or perform lateralized movements (Grillner and Matsushima, 1991; Talpalar et al., 2013; Dunn et al., 2016; Koyama and Pujala, 2018). For asymmetrical activation of the bilateral CNS, the reciprocal inhibition between the left and right sides is believed to play a key role (Beaulé et al., 2012; Palmer et al., 2012). Despite, however, the importance of reciprocal inhibition in the control of vertebrate

Received Aug. 1, 2018; revised Dec. 13, 2018; accepted Dec. 16, 2018.
Author contributions: T.S., Y.O., and S.-i.H. wrote the first draft of the paper; T.S., M.T., Y.O., and S.-i.H. edited the paper; T.S., Y.O., and S.-i.H. designed research; T.S. performed research; M.T. contributed unpublished reagents/analytic tools; T.S. analyzed data; T.S., Y.O., and S.-i.H. wrote the paper.
This work was supported in part by Ministry of Education, Culture, Sports, Science and Technology of Japan Grants 25250002 and 16K06991 to Y.O. We thank Dr. Azusa Kamikouchi and Dr. Tsunehiko Kohashi for continuous encouragement and discussion; Yurie Matsutani, Hiroko Ito, Yoko Terasawa, and Yoshiko Takeuchi for fish care; and Spectrography and Bioimaging Facility of the National Institute for Basic Biology Core Research Facilities for providing technical support.
The authors declare no competing financial interests.

Correspondence should be addressed to Yoichi Oda at oda@bio.nagoya-u.ac.jp or Shin-ichi Higashijima at shigashi@nibb.ac.jp.
https://doi.org/10.1523/JNEUROSCI.1964-18.2018
 0270-6474/19/391182-13$15.00/0

behaviors, the identification of reciprocal inhibition circuits at the individual cell level and the contribution of each neuron to the asymmetric activity are still quite limited (Moult et al., 2013; Roberts et al., 2014), largely because multiple circuits may participate in shaping motor output, making it difficult to identify neurons of the circuits and to evaluate how each neuron contributes to producing these movements.

The fast escape response of teleost fish to abrupt stimuli provides a typical lateralized behavioral model for investigating network organization and the function of reciprocal inhibition (Faber et al., 1989; Korn and Faber, 2005) because the principal circuits from sensory inputs to motor outputs are simple and identifiable and the behavior is basic enough that it is possible to evaluate the contribution of the key neurons. A pair of giant reticulospinal neurons in the hindbrain, Mauthner (M) cells, are known to trigger the escape, especially in response to sound/vibration stimuli (Zottoli, 1977; Eaton et al., 1981; Burgess and Granato, 2007; Kohashi and Oda, 2008). When one of the paired M cell fires, it directly or indirectly activates the spinal motoneurons of the contralateral trunk muscles (Yasargil and Diamond, 1968). Thus, the single spiking of an M cell induces the contraction of trunk muscle exclusively along the axis on the contralateral side, resulting in a C-shaped body bend (C bend) at the initial phase of escape. However, sound/vibration stimuli could activate both M cells because it is received by both ears directly as well as through the swim-bladder. Nevertheless, fish exhibit a C bend and escape to one direction reliably. For that to occur, it has been believed that two types of reciprocal inhibition at the level of the hindbrain and spinal cord play critical roles in activating only one side and inhibiting the contralateral side (Diamond, 1971). Actually, the commissural interneurons in the spinal cord identified in goldfish (Fetcho and Faber, 1988), tench (Yasargil and Sandri, 1990), and larval zebrafish (named "CoLo") (Satou et al., 2009) are activated directly by the M cell and strongly inhibit the contralateral spinal neurons, even when the contralateral M cell fired after the first M cell (Satou et al., 2009). At the hindbrain level, there is a reciprocal inhibition between M cells (Furukawa and Furshpan, 1963) that is mediated by cranial relay neurons (CRNs) (Hackett and Faber, 1983b; Koyama et al., 2011) that receive excitatory inputs from M axons and excite glycinergic interneurons contacting the contralateral M cell. The role of the reciprocal inhibition for M cell excitability and escape behavior, however, is unclear because the number and location of CRNs that mediate the reciprocal inhibition are unknown. In the present study, we identified two paired CRNs in a GFP-expressing transgenic line of zebrafish larvae and examined the effects of their elimination on M cell firing and sound/vibration-evoked escape behavior. We show the following: (1) two paired CRNs located in the posterior hindbrain largely mediate the reciprocal inhibition of M cells; and (2) the reciprocal inhibition plays a critical role in preventing bilateral firing of M cells, thereby allowing for full flexion of the C bend during escape.

Materials and Methods

Animals. Zebrafish adults, embryos, and larvae were maintained at 28.5°C. Experiments were performed at room temperature (23°C–28°C). All procedures were performed in compliance with the guidelines approved by the animal care and use committees of the National Institutes of Natural Sciences and Nagoya University. Animals were staged according to days post fertilization (dpf).

The Tol-056 enhancer trap line in which GFP is expressed in M cells and several classes of interneurons (Satou et al., 2009; Tanimoto et al., 2009) were used to identify two rostrally located T reticular neurons, Ta1 and Ta2. *nacre* mutants that lack black pigment cells were used in many of the experiments for easier identification of Ta1 and Ta2 neurons. The immotile mutant fish *relaxed* (*relaxed*^{mi90}) (Zhou et al., 2006) was used for electrophysiological studies.

Retrograde labeling of T reticular neurons. Four- to five-day-old Tol-056 larvae were anesthetized with 0.02% tricaine methanesulfate (MS-222; Sigma-Aldrich) and placed on an agarose plate. Then, 10% tetramethyl-rhodamine-dextran (10,000 MW; Thermo Fisher Scientific) was pressure-injected into the rostral spinal cord or the midbrain near the midline (Kimmel et al., 1985). After the injection, the larvae were allowed to recover in 10% Hanks solution for >4 h. The larvae at 5 dpf were then mounted on low-melting point agarose (1.5%; Thermo Fisher Scientific) in glass-bottomed 35 mm plastic dishes and viewed with a confocal microscope (TCS SP8; Leica Microsystems).

Electroporation of rhodamine-dextran into single cells. Single-cell labeling of Ta1 and Ta2 with tetramethyl-rhodamine-dextran by electroporation was performed essentially as described previously (Bhatt et al., 2004; Kimura et al., 2006). The dissection procedures of the samples were the same as those for electrophysiology (see Electrophysiology). Labeled neurons were viewed with a confocal microscope as described above.

Electrophysiology. In vivo whole-cell recordings were performed as described previously (Watanabe et al., 2014, 2017) with some modifications. M cells are known to be cholinergic (Koyama et al., 2011). To paralyze the fish without blocking the cholinergic transmission, we used the *relaxed* mutants, which have a nonsense mutation in the skeletal muscle dihydropyridine receptor *cacnb1*, resulting in defective excitation–contraction coupling in skeletal muscles (Zhou et al., 2006; Koyama et al., 2011). We dechorionated the homozygous mutants at 2 dpf and used them at 5 dpf. The 5 dpf larvae were anesthetized with MS-222 and then rinsed and pinned with tungsten wires on a silicon dish filled with extracellular solution (134 NaCl, 2.9 KCl, 2.1 $CaCl_2$, 1.2 $MgCl_2$, 10 HEPES, and 10 glucose, 290 mOsm, adjusted to pH 7.8 with NaOH). The head skin was peeled off, and a thin layer of dorsal hindbrain was removed by suction through a glass pipette (diameter >10 μm) to allow access to M cells and Ta1/Ta2 neurons. Whole-cell recordings from M cells or Ta1/Ta2 neurons were obtained with a MultiClamp 700B amplifier (Molecular Devices) and were collected on a computer using a digitizer (Digidata 1440A, Molecular Devices). Patch-clamp electrodes were pulled from borosilicate glass (GD-1.5; Narishige) with a pipette resistance of 4–6 MΩ for M cell and 9–10 MΩ for Ta1/Ta2 neurons. Intracellular solution contained the following (in mM): 119 K-gluconate, 6 KCl, 2 $MgCl_2$, 10 HEPES, 10 EGTA, and 4 Na_2 ATP at 290 mOsm and adjusted to pH 7.2 with KOH. The calculated liquid junction potential was 15 mV, which we corrected for. When eliciting action potentials in the M cell or Ta1/Ta2 neurons, we set the strength of the current near the threshold: with the current injections of the same amplitude, action potentials occurred in some trials, but not in other trials.

Loose-patch recordings from paired M cells were performed as described previously (Kimura et al., 2013). During the recordings, sinusoidal stimulus waveforms (500 Hz, 2 cycles) were generated by a function generator (DF 1906; NF), amplified by an audio amplifier (R-810M; Onkyo), and delivered to the audio speaker (K36WP, 3.6 cm in diameter; Visaton), which was attached to the bottom of the microscope stage using dental wax (see Fig. 7*A*).

Laser ablation. Laser ablation of Ta1, Ta2, Mauthner, or CoLo neurons was performed in 2 or 3 dpf larvae of the Tol-056 enhancer trap line. Larvae were anesthetized and embedded in 1.5% low melting-point agarose (Thermo Fisher Scientific). Then, the sample was placed under the multiphoton microscope (Leica Microsystems, TCS SP8 MP). Ta1 and Ta2 neurons were unilaterally or bilaterally photo-ablated using a two-photon laser (wavelength 900 nm). In some cases, CoLo neurons or M cells were also photo-ablated in addition to Ta1/Ta2. Scanning was immediately terminated when brief flashes of saturating intensity were observed, which are thought to be created by a highly localized plasma caused by photon absorption by water molecules (Orger et al., 2008). After the ablation, larvae were allowed to recover until 5 dpf and were then used for electrophysiological or behavioral experiments. Successful ablations were verified during (in electrophysiological recordings) or after (in behavioral experiments) the experiments by checking for the absence of GFP fluorescence.

Calcium imaging. Calcium imaging of M cells was performed essentially as described previously (Kohashi and Oda, 2008; Satou et al., 2009), except that a red fluorescent calcium indicator, Cal-590 dextran (10,000 MW; AAT Bioquest), was used instead of Calcium Green dextran. This was because we used Tol-056 strains in which M cells expressed GFP.

After the injection of Cal-590 dextran at 4 or 5 dpf, larvae were allowed to recover in 10% Hanks solution for >6 h. Larvae at the age of 5 dpf were then mounted on low-melting point agarose (1.5%; Thermo Fisher Scientific) in glass-bottomed 35 mm plastic dishes in an upright position. The dish was then attached to the sound/vibration stimulation apparatus (the same one used for the behavioral experiments; see below) with an orientation such that the head faced toward the audio speaker (Satou et al., 2009). The setting was placed on a BX51WI upright microscope (Olympus) equipped with a spinning-disk confocal unit (CSU-X1; Yokogawa). A 20× water-immersion objective (numerical aperture, 1.0) was used for the observations. The illumination laser was a 561 nm DPSS laser (DPL561; Cobolt). In some cases, wide-field illumination with a mercury lamp and mCherry filter set (Semrock) was used. In these cases, the spinning-disk confocal unit was removed from the microscope. For image acquisition, an ORCA-Flash 4.0 camera and HCImage software (Hamamatsu Photonics) were used with a frame rate of 200 ms/frame.

We used larvae of the Tol-056 line under WT background or *relaxed* background. Approximately half of the data were collected using *relaxed* fish (both for control and Ta1/Ta2-ablated fish). Because data obtained from WT and *relaxed* backgrounds were not significantly different, we pooled the data.

Behavioral analyses. Behavioral experiments were performed as described previously (Satou et al., 2009; Kohashi et al., 2012; Takahashi et al., 2017) using 5 dpf larvae. Briefly, we used a custom-made sound/vibration stimulation system to elicit escape behavior. A glass Petri dish 30 mm in diameter was tightly attached to the platform by dental wax. The vibration platform consisted of an audio speaker (FRS8, 7 cm in diameter; Visaton) attached to an acrylic plate (see Fig. 6*A2*). The stimulation signal (500 Hz, 2 cycles) was delivered to the audio speaker as described above. Three larval fish were tested in every experiment after 20 min of acclimation. Sequential images of the escape responses were captured at 1000 frames/s by a high-speed camera (FASTCAM-ultima1024; Photron) at 1024 × 1024 pixel resolution. Responses with latency <15 ms were considered escapes and analyzed (Burgess and Granato, 2007; Satou et al., 2009). In a minority of cases, larvae started spontaneous movements before the arrival of the sound/vibration stimuli. These trials were excluded from the data analyses. Successive trials were separated by at least 2 min. The amplitude of escape bend was measured by the angle change of the rostral midline (nose to swim bladder) after the onset of the response.

Behavioral experiments in head-fixed larvae were essentially the same as those described by Kohashi and Oda (2008) and Kimura et al. (2013). Briefly, larvae at 5 dpf were mounted in low-melting-point agarose (1.5%–2.0%, Thermo Fisher Scientific). Agarose covering the tail part was removed so that the tail could move. The cutting position was set at three segments rostral to the cloaca. Movements of the animals were monitored from the bottom using a 2× objective lens (Olympus) with infrared LED illumination and recorded using the high-speed camera. The tail flexion angle was measured using the two body positions on the midline. Position 1 was set at the edge of the agar (three segments rostral to the cloaca). Position 2 was set at a quarter length of the free-tail part. The line between the two positions at the time frame of 8 ms after the onset of the movement was drawn. Then, the angle between this line and the body line before the movement was determined manually. Determination of Position 2 at the time frame of 8 ms was aided by the pigmentation patterns of xanthophores that were clearly visible with infrared illumination.

Statistics. Results are presented as mean ± SEM. The statistical significance was assessed using the Mann–Whitney *U* test, Wilcoxon signed-rank test, Kolmogorov–Smirnov test, or *t* test. For the *t* test, we checked the normality of the distributions by the Shapiro–Wilk test ($p > 0.05$) and the equality of the variance with the *F* test ($p > 0.05$).

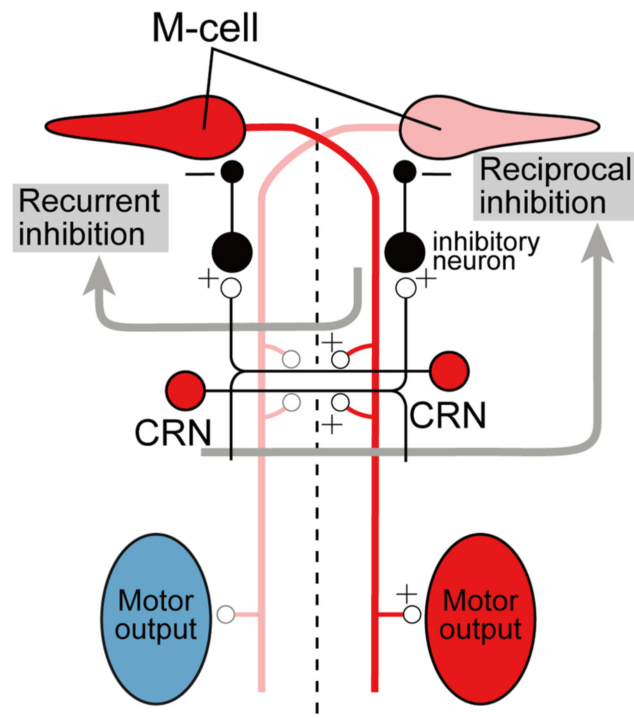

Figure 1. Reciprocal and recurrent inhibitory pathways of the M-cell network. Dorsal view with rostral to the top (the same is true for all subsequent figures). This figure assumes that the left M cell fires. The output of the left M cell is relayed through CRNs: CRNs located on both sides are excited (cells labeled in red). The left CRN excites a class of inhibitory neurons on the right side (black cell on the right). These inhibitory neurons provide inhibition to the right M cell (reciprocal inhibition). The right CRN excites the same class of inhibitory neurons on the left side (black cell on the left). These neurons provide inhibition to the left M cell (recurrent inhibition). In the spinal cord, the M spike running on the right side excites motoneurons, leading to an escape bend to that side (red oval labeled as "motor output"). There is no motor output on the other side (blue oval).

Results

Before describing the results, we need to summarize what is known about reciprocal and recurrent inhibition pathways in the M-cell network. Firing of an M cell evokes short-latency glycinergic inhibition both to the same M cell (recurrent inhibition in Fig. 1) and to the M cell on the contralateral side (reciprocal inhibition in Fig. 1) (Furukawa and Furshpan, 1963; Faber and Korn, 1978; Faber et al., 1989). In both cases, the outputs of the M cell are relayed by a class of excitatory neurons called CRNs (Hackett and Faber, 1983b; Hackett et al., 1989). The CRNs are commissural neurons that excite a class of inhibitory neurons, which in turn inhibit M cells (Fig. 1). The CRN is monosynaptically excited by the M axons running on both sides of the CNS. In this configuration, the pathway excited by the ipsilaterally running M axon (contralateral soma) is involved in recurrent inhibition, whereas the pathway excited by the contralaterally running M axon (ipsilateral soma) is involved in reciprocal inhibition (Fig. 1). Thus, one CRN is involved in either reciprocal or recurrent inhibition, depending on which M cell fires.

The Tol-056 enhancer trap line labels two rostrally located T reticular neurons, Ta1 and Ta2

Although the overall configuration of the reciprocal/recurrent inhibition pathway of the M cells has been identified (Fig. 1), the exact numbers and location of CRNs are unknown in classical electrophysiological studies. Separate anatomical evidence suggests that CRNs overlap with a subset of (or possibly all) T

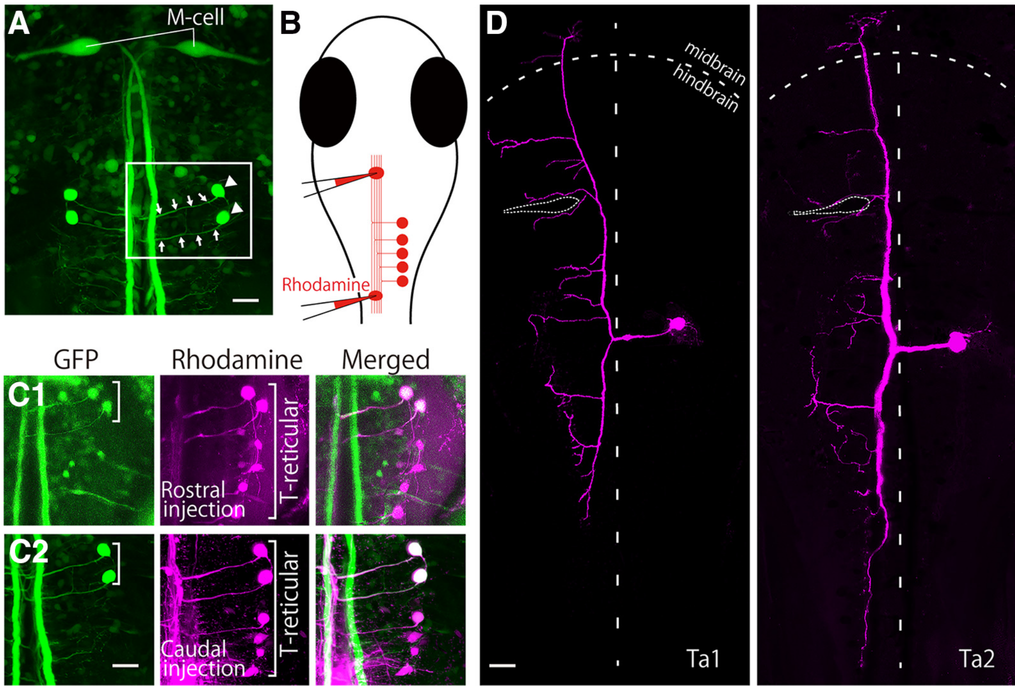

Figure 2. The Tol-056 enhancer trap line labels two rostrally located T reticular neurons. ***A***, Stacked image of confocal optical sections of a 5 dpf larva. GFP expression is present in a pair of M cells in the hindbrain. In addition, GFP is expressed in a pair of two relatively large neurons (12–13 μm in diameter) in the caudal hindbrain (arrowheads). Prominent commissural axons arise from these two cells (arrows). ***B***, Schematic illustration of retrograde labeling for the visualization of T reticular neurons. ***C1***, ***C2***, Retrograde labeling of T reticular neurons in the Tol-056 line. ***C1***, Results of the rostral injection. ***C2***, Results of the caudal injection. In both cases, two GFP-expressing cells overlap with the most rostrally located T reticular neurons (arrays of longitudinally aligned neurons). ***D***, Morphology of individual Ta1 (left) and Ta2 (right) neurons, revealed by electroporation of tetramethyl rhodamine dextran. Fine dotted lines indicate the location of M cells. Coarse dotted lines indicate the midbrain-hindbrain boundary and midline. Scale bar, 20 μm.

reticular neurons. T reticular neurons are arrays of longitudinally aligned neurons located in the caudal hindbrain with prominent soma and crossed T-shaped axons, both of which can be identified by retrograde-dye filling (Kimmel et al., 1985) (Fig. 2*B*,*C*). Koyama et al. (2011) indeed showed that some T reticular neurons identified by retrograde-dye filling corresponded to CRNs.

Toward the reproducible and simpler identification of CRNs, we looked for enhancer/gene trap lines in which GFP was expressed in neurons having morphologies characteristics of T reticular neurons. One enhancer trap line we noticed was Tol-056. In the enhancer trap line, GFP is reported to be expressed in M cells and a class of inhibitory neurons called CoLo located in the spinal cord (Satou et al., 2009). In addition to these cells, we noticed that GFP is expressed in two relatively large neurons (12–13 μm in diameter) in the caudal hindbrain (Fig. 2*A*, arrowheads). Prominent commissural axons arose from these two cells (Fig. 2*A*, arrows). The morphology of the cells resembles that of T reticular neurons (Kimmel et al., 1985), leading us to speculate that a subset of T reticular neurons are labeled by GFP in the Tol-056 line. To test this supposition, we performed retrograde labeling in Tol-056 fish. Rhodamine dye was injected either into the caudal midbrain or the rostral spinal cord (Fig. 2*B*; $n = 2$ for the rostral injection; $n = 3$ for the caudal injection). In both cases, two GFP-expressing cells overlapped with the most rostrally located T reticular neurons (Fig. 2*C1*,*C2*). These results indicate that the Tol-056 line labels two of the most rostrally located T reticular neurons. We named these two neurons Ta1 (the rostral one) and Ta2 (the caudal one). Caudally to Ta2, ~5 T-reticular neurons (we named them the Tp neurons) were retrogradely labeled on the contralateral side of the rhodamine injection, as described previously (Kimmel et al., 1985). It should be noted that round-shaped somata of Ta1 ($108.5 \pm 0.9\ \mu m^2$, range 95.1–120.6 μm^2, $n = 5$) and of Ta2 ($111.7 \pm 9.0\ \mu m^2$, range 86.6–132.6 μm^2, $n = 5$) are significantly larger ($p = 0.00000623$ and 0.00000915, respectively, t test) than those of Tp ($62.2 \pm 3.8\ \mu m^2$, 37.9–92.5 μm^2, $n = 19$), as represented by the projection area of the stacked images. Next, we investigated the morphology of Ta1 and Ta2 neurons by performing electroporation of rhodamine dye into individual Ta1 and Ta2 neurons ($n = 3$ for each cell). Figure 2*D* shows a representative example of Ta1 (left) and Ta2 (right). For both Ta1 and Ta2 neurons, a prominent commissural axon arose from the soma. After crossing the midline, the axon bifurcated, with one extending rostrally and the other extending caudally. Along the way, the axon exhibited extensive innervation in the contralateral hindbrain. The rostral-most axon extended to the midbrain. The overall morphology of Ta1 and Ta2 neurons was very similar to that of the CRNs previously revealed by electrophysiological studies coupled with dye filling (Hacket and Faber, 1983a; Koyama et al., 2011). It should be noted that there was a difference in the extent of the caudal axon between Ta1 and Ta2: the caudally extending axon of Ta1 was shorter than that of Ta2 (Fig. 2*D*). This feature was consistently observed for two of the cells of each type.

Electrophysiological studies of Ta1 and Ta2 neurons

Having shown that Ta1 and Ta2 neurons have morphological features that fulfill CRNs, we then examined whether they indeed had functions of CRNs by performing whole-cell electrophysiological recordings from each of these cells together with the M cell. If these cells correspond to CRNs, they should receive direct excitatory inputs from the M cell located both on the ipsilateral and contralateral sides (Fig. 1). In addition, the firing of each cell should evoke IPSPs in the M cell located on the contralateral side

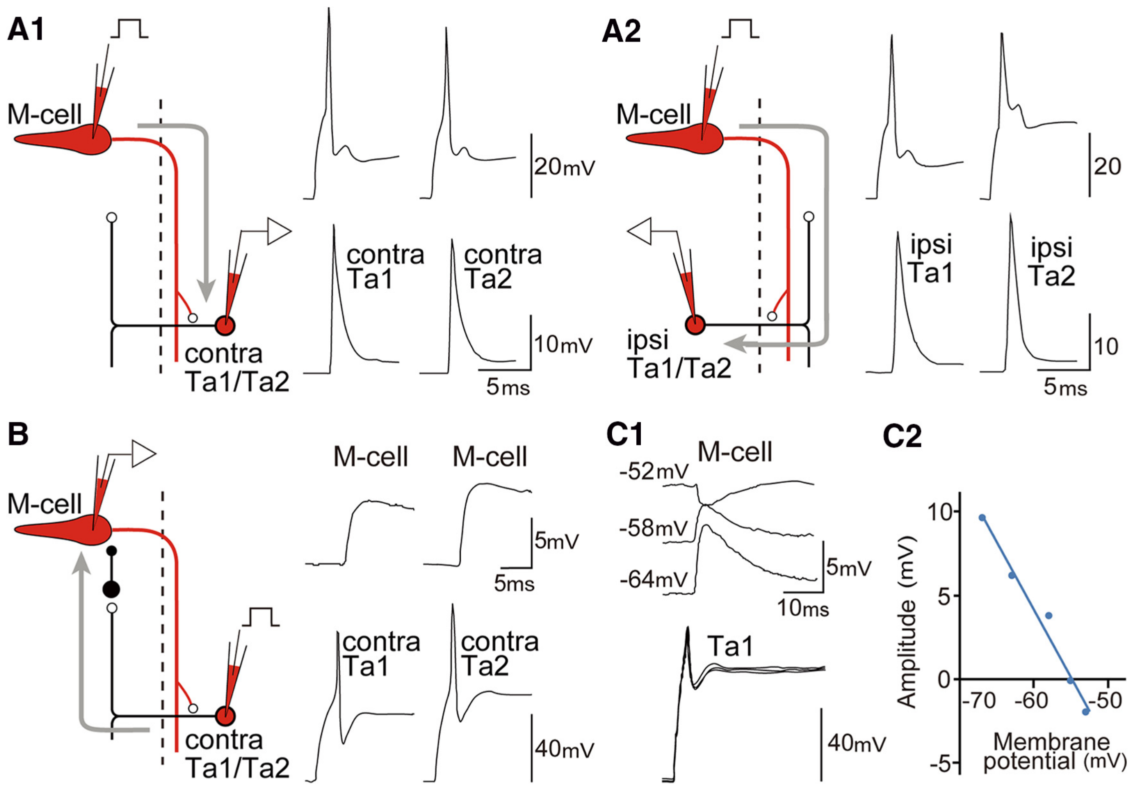

Figure 3. Electrophysiological recordings from the M cell and Ta1/Ta2 neurons. ***A1***, Paired recording between the M cell and the Ta1/Ta2 neuron on the contralateral side. A square current was injected into the M cell to elicit an action potential, and the response in a Ta1 or a Ta2 neuron was recorded (left). Both for Ta1 (middle) and Ta2 (right), a firing of the M cell evoked a spike-like steep voltage increase. ***A2***, Paired recording between the M cell and the Ta1/Ta2 neuron on the ipsilateral side. A square current was injected into the M cell to elicit an action potential, and the response in a Ta1 or a Ta2 neuron was recorded (left). Both for Ta1 (middle) and Ta2 (right), a firing of the M cell evoked a spike-like steep voltage increase. ***B***, Paired recording between the Ta1/Ta2 neuron and the M cell on the contralateral side (left panels). A square current was injected into the Ta1 or Ta2 neuron to elicit an action potential (bottom panels), and the response in the M cell was recorded (top panels). ***C1***, Recordings between the T1 neuron and the M cell on the contralateral side. The M cell was held at several different membrane potentials by injecting positive currents. The amplitude of the PSPs depended on the holding membrane potentials. ***C2***, Plots showing the relationship between PSP amplitudes and holding membrane potential of the M cell. The PSP reversed near −54 mV, which approximately corresponds to the calculated chloride reversal potential.

(Fig. 1). We tested whether these connections existed between Ta1/Ta2 and the M cell.

Figure 3*A1* shows representative examples of the paired recordings between the M cell and Ta1/Ta2 on the contralateral side. A square current was injected into the M cell to elicit an action potential, and the response in a Ta1 or a Ta2 neuron was recorded (Fig. 3*A1*, left). Both for the Ta1 (Fig. 3*A1*, middle) and Ta2 (Fig. 3*A1*, right), a firing of the M cell (top traces) led to a spike-like steep voltage increase with the amplitude exceeding 20 mV (bottom traces). We speculate that the response was a spike that was back-propagated to the recording site: in CRNs, an M cell-evoked spike is supposed to occur near the contact sites between the M axon and the axon of a CRN (Fig. 1). For each Ta1 and Ta2, we obtained three paired recordings between the cell and the M cell and essentially obtained the same results. The latency of the responses was always very short (0.4–0.6 ms) and consistent for all the recordings. This is compatible with the idea that the sharp responses were monosynaptically induced ones.

Figure 3*A2* shows a representative example of the connections between the M cell and Ta1/Ta2 on the ipsilateral side. We essentially obtained the same results that were seen for the T1/Ta2 on the contralateral side: a current-induced spike of the M cell evoked a short-latency spike-like response of the Ta1/Ta2 on the ipsilateral side ($n = 3$ for Ta1; $n = 3$ for Ta2; latency, 0.4–0.6 ms for all the recordings).

We then tested whether firing of Ta1/Ta2 led to responses in the M cell on the contralateral side (Fig. 3*B*, left). For both Ta1

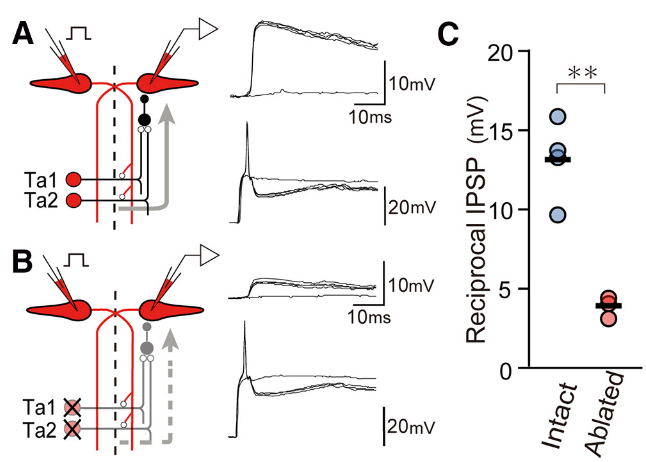

Figure 4. Reciprocal inhibition is significantly reduced in the absence of Ta1 and Ta2 neurons. ***A***, Paired recording between the two M cells in an intact animal. Left, Schematic of the recording. A square current was injected into one of the M cells to elicit an action potential (bottom right), and the response of the other M cell was recorded (top right). Four traces are superimposed. In one trace, an action potential was not elicited. ***B***, Paired recording between the two M cells in an experimental animal. In this animal, Ta1 and Ta2 neurons on the left side were unilaterally ablated (left). Broken line with an arrow indicates that the reciprocal inhibition would be reduced under these conditions. A square current was injected into the left M cell to elicit an action potential (bottom right), and the response of the right M cell was recorded (top right). In one trace, an action potential was not elicited. ***C***, Population data of the amplitude of the reciprocal IPSPs ($n = 4$ for the intact animals; $n = 3$ for the ablated animals). Each circle represents the average IPSP of 1 animal (for each animal, three responses were averaged). Horizontal black lines indicate averages of the intact (left) and the ablated (right) animals. $^{**}p < 0.01$ (*t* test).

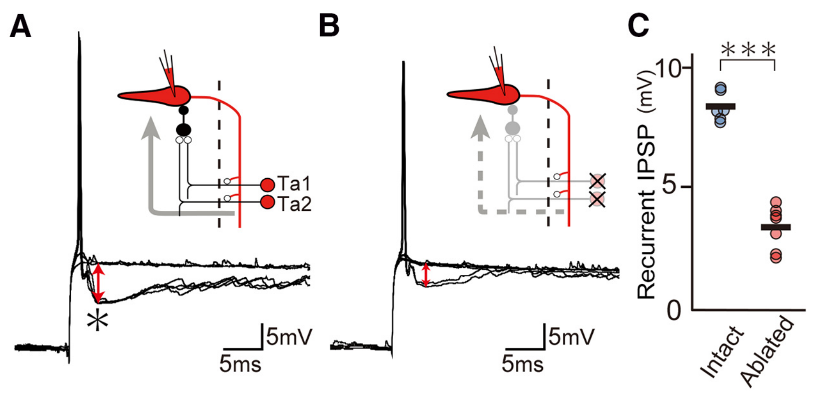

Figure 5. Recurrent inhibition is significantly reduced in the absence of Ta1 and Ta2 neurons. ***A***, Recording from the M cells in an intact animal. Top right, Schematic illustration of the recording. A square current was injected into the M cell to elicit an action potential. Four traces are superimposed. In one trace, no action potential occurred. Using this trace as a reference, the amplitude of recurrent IPSPs (double-headed red arrow marked by an asterisk) was measured. ***B***, Recording from the M cells in an experimental animal. Top right, Schematic illustration of the recording. The Ta1 and Ta2 neurons contralateral to the recorded M cell were ablated. Broken line with an arrow indicates that the recurrent inhibition would be reduced in this condition. The amplitude of recurrent IPSPs (double-headed red arrow) was measured as described above. ***C***, Population data of the amplitude of recurrent IPSPs ($n = 8$ for the intact animals; $n = 7$ for the ablated animals). Each circle represents the average IPSP of 1 animal (for each animal, three responses were averaged). Horizontal black lines indicate averages of the intact (left) and the ablated (right) animals. $^{***}p < 0.001$ (Mann–Whitney *U* test).

and Ta2 (Fig. 3*B*, right), current-induced action potentials of these cells (bottom traces) resulted in depolarizing postsynaptic potentials (PSPs) in the M cell (top traces, $n = 3$ for Ta1; $n = 3$ for Ta2). We speculated that these depolarizing PSPs were inhibitory PSPs (IPSPs) because, in our recording condition with the chloride-reversal potential being −52 to −53 mV, IPSPs were expected to be recorded as a depolarizing response (the resting membrane potential of the M cell was ∼−70 mV). To confirm that the observed PSPs were IPSPs, we recorded the responses in the M cell with various membrane potentials by injecting positive currents. As shown in Figure 3*C1* (the result of Ta1; similar results were obtained for Ta2), the responses in the M cell depended on the holding membrane potentials. With the higher membrane potential, the depolarizing response became smaller, and reversed near the calculated reversed potential of the chloride ion (−54 mV) (Fig. 3*C2*), indicating that the observed PSPs in the M cell were indeed IPSPs. The latency of the IPSPs in the M cell ranged from 1.2 to 1.8 ms for all the recordings, which was consistent with the idea that the IPSPs were evoked by disynaptic connections (Fig. 3*B*, left).

In summary, the results of the paired electrophysiological recordings confirmed that both Ta1 and Ta2 neurons correspond to CRNs that were previously characterized (Hacket and Faber, 1983b; Koyama et al., 2011).

Ta1 and Ta2 neurons account for a large part of reciprocal/recurrent inhibition in the M-cell network

Next, we investigated the extent of the contribution of Ta1 and Ta2 for the reciprocal and recurrent inhibition in the M-cell network. For this purpose, we laser-ablated both the Ta1 and Ta2 neurons, and recorded the amplitude of reciprocal or recurrent IPSPs in the M cell: if Ta1 and Ta2 constitute a major part in the pathway, the recorded amplitude of IPSPs would be greatly reduced compared with that of control animals.

For examining reciprocal IPSPs, we performed paired recordings from the two M cells. In control animals, the firing of one M cell led to the depolarizing IPSP in the M cell on the contralateral side with the amplitude ∼14 mV (Fig. 4*A*). When the same experiment was performed in the animal where the Ta1 and Ta2 were unilaterally ablated (Fig. 4*B*), the amplitude of the IPSPs recorded in the contralateral M cell was significantly smaller than that of the control animal (compare Fig. 4*A* with Fig. 4*B*). Figure 4*C* shows population data. The average IPSP amplitude in the control animals ($n = 4$) was 13.1 ± 1.2 mV, whereas that in the experimental animals ($n = 3$) was 3.8 ± 0.4 mV ($p = 0.00188$, *t* test). These results indicate that Ta1 and Ta2 account for a major part (∼71%) of relay functions. The results also indicate that there are CRNs other than Ta1 and Ta2 because reciprocal IPSPs were not completely abolished in the absence of Ta1 and Ta2.

We then examined recurrent IPSPs. In control animals, the firing of an M cell led to IPSPs in the same neuron with the amplitude ∼8 mV (Fig. 5*A*, red-colored double-headed arrow marked by an asterisk): the amplitude of the IPSPs was measured using the nonfiring trace as the reference. When the same experiment was performed in the animal where the Ta1 and Ta2 on the contralateral side were unilaterally ablated (Fig. 5*B*), the amplitude of the IPSPs recorded in the M cell was significantly smaller than that of the control animal (compare Fig. 5*A* with Fig. 5*B*). Figure 5*C* shows population data. The average IPSP amplitude in the control animals ($n = 8$) was 8.4 ± 0.2 mV, whereas that in the experimental animals ($n = 7$) was 3.1 ± 0.3 mV ($p < 10^{-3}$, Mann–Whitney *U* test). These results indicate that Ta1 and Ta2 account for a major part (∼63%) of relay functions. The results also indicate that there are CRNs other than Ta1 and Ta2 because recurrent IPSPs were not completely abolished in the absence of Ta1 and Ta2.

Collectively, the results of the Ta1/Ta2 ablation experiments indicate that Ta1 and Ta2 play a major role in relay functions for producing reciprocal as well as recurrent IPSPs.

Calcium imaging of the M cells in the animals in which Ta1 and Ta2 neurons are ablated

Next, we examined whether the reduction of reciprocal/recurrent inhibition with the ablation of Ta1 and Ta2 would affect activity patterns of the M cells upon sudden sound/vibration stimuli. For observing activity patterns of the M cell, we performed calcium imaging (O'Malley et al., 1996; Takahashi et al., 2002; Kohashi and Oda, 2008; Satou et al., 2009). The M cells were retrogradely labeled with a red fluorescent Ca^{2+} indicator, Cal-590 dextran (Fig. 6*A1*), and imaged with confocal microscopy. The red fluorescent dye was used because M cells were labeled by GFP in the Tol-056 line that was used in the experiments. The sound/vibration stimuli with little laterality were delivered to the animals as described previously (Satou et al., 2009) (Fig. 6*A2*).

As described by Satou et al. (2009), the stimulus evoked unilateral (Fig. 6*B*) or bilateral (Fig. 6*C*) activations of the M cells. The responses in each M cell occurred in an all-or-nothing manner with steady amplitudes. This response was shown to correspond to one action potential of the M cell (Kohashi and Oda, 2008; Satou et al., 2009). We asked whether the probability of the bilateral activations of the two M cells would be increased in the animals in which the Ta1 and Ta2 neurons were bilaterally ablated (Fig. 6*D*,*E*). Figure 6*F* (control animal) and Figure 6*G* (experimental animal) show representative examples of traces of the two M cells in successive trials. Traces in blue show those of unilateral activations, whereas traces in red show those of bilateral activations. Traces in gray show those of no activations (stimulus strength was set such that responses occurred in ~70%–80% of trials). In the control animal (Fig. 6*F*), the probability of bilateral activations was 36% (4 of 11; trials of no activation were excluded from the calculation), which was comparable with that of the previous study (Satou et al., 2009). In contrast, in the experimental animal (Fig. 6*G*), the probability of bilateral activations was hugely increased to 75% (9 of 12), a value that was not observed in the previous study (Satou et al., 2009). Figure 6*H* shows population data, which include the results of 8 control animals and 7 experimental animals. The average probability of the bilateral activations was significantly increased (41.8% for the control animals and 75.4% for the experimental animals) ($p < 10^{-3}$, Mann–Whitney *U* test). These results indicate that, under the conditions of the reduced reciprocal inhibition by the bilateral ablations of Ta1 and Ta2 neurons, the probability of coactivations of the two M cells was significantly increased.

The ablations of Ta1 and Ta2 neurons not only reduce reciprocal inhibition but also recurrent inhibition, which might lead to successive firings of the same M cell. If this occurs, we would see responses with a significantly larger amplitude, an indication of successive firings in the M cell (Takahashi et al., 2002). Throughout the experiments, however, the amplitude of the responses was stable both in the control animals and in the experimental animals. This indicates that successive firings of the same M cell did not occur in the animals in which Ta1 and Ta2 neurons were bilaterally ablated (see Discussion).

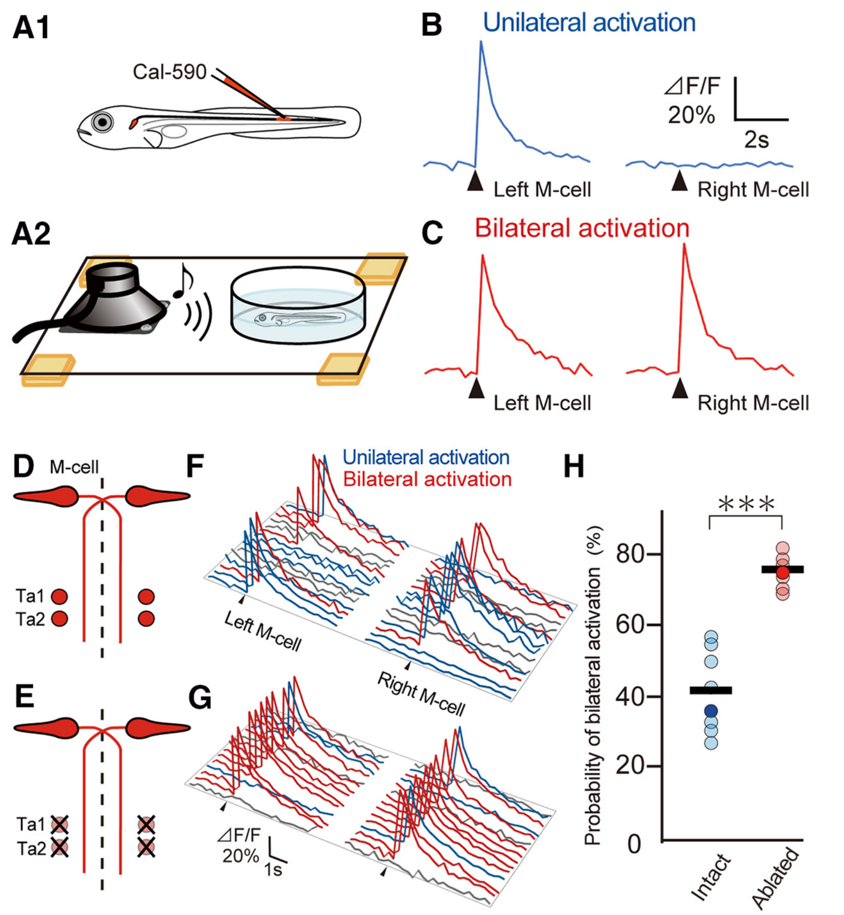

Figure 6. Calcium imaging of M cells. ***A1***, Dextran-conjugated Cal-590 indicator was injected into the spinal cord of larvae of the Tol-056 line to label the M cells with the dye. ***A2***, Schematic illustration of the apparatus to deliver a sound/vibration stimulus to the animal. ***B***, ***C***, Examples of fluorescent responses in the M cells of an intact animal. As shown in a previous study (Satou et al., 2009), unilateral activation (***B***, blue traces) or bilateral activation (***C***, red traces) occurred. ***D***, ***E***, Schematic illustrations of the ablation design. ***D***, Control (intact) conditions. In an experimental animal shown in ***E***, Ta1 and Ta2 on both sides were ablated. ***F***, ***G***, Traces of the two M cells in successive trials in a control (***F***) and an ablated (***G***) animal. Blue traces indicate those of unilateral activations. Red traces indicate those of bilateral activations. Gray traces indicate those of no activations. In the ablated animal, the probability of the bilateral activations is much higher than that in the control animal. In all the trials, the responses of each M cell occurred in an all-or-nothing manner with steady amplitudes. ***H***, Population data of the probability of bilateral activations ($n = 8$ for the control animals and $n = 7$ for the ablated animals). Trials of no activation were excluded from the calculation. Data exemplified in ***F*** and ***G*** are shown by dark marks. Horizontal black lines indicate averages of the intact (left) and the ablated (right) animals. ***$p < 0.001$ (Mann–Whitney *U* test).

Electrophysiological recordings of the M cells in the animals in which Ta1 and Ta2 neurons are ablated

Previous studies suggest that coactivations of the two M cells in control animals occur with a time difference of the two M cell spikes being within ~2 ms (Takahashi et al., 2002; Satou et al., 2009). This narrow time window corresponds to the necessary time for the reciprocal inhibition (disynaptic pathway) to take place. Considering this, the increase of coactivations (~35% increase) observed by calcium imaging in the animals with Ta1 and Ta2 neurons ablated (Fig. 6) is likely to be caused by the occurrences of those bilateral activations with which the time difference of the two M cell spikes exceeded this time window.

To confirm this notion, we performed loose-patch electrophysiological recordings from two M cells to determine spike timings upon the sound/vibration stimulations (Fig. 7*A*). Figure 7*B1* and Figure 7*B2* are representative examples of spike responses of the two M cells in intact and Ta1/Ta2-ablated animals, respectively. Time differences of the two spikes in the intact animals (three fish) were mostly within 2 ms, ranging from 0.11 to 2.54 ms ($n = 32$) (Fig. 7*C*). By contrast, in the case of the Ta1/Ta2-ablated animals (3 fish), they indeed often exceeded 2 ms, ranging from 0.01 to 4.03 ms ($n = 33$) (Fig. 7*C*). In Figure 7*D*, the population data of the two groups are shown as a histogram. This clearly shows the difference of the distributions ($p = 0.003$, two-sample Kolmogorov–Smirnov test), thus confirming this notion. It should be noted that the increase in probability of the bilateral M-cell activation was also observed in the electrophysiological recordings (33.2% in the intact fish; 70.7% in the Ta1/Ta2-ablated fish).

Behavioral experiments in the animals in which Ta1 and Ta2 neurons are ablated

Next, we investigated whether the reduced reciprocal inhibition with the ablation of Ta1 and Ta2 would affect an animal's

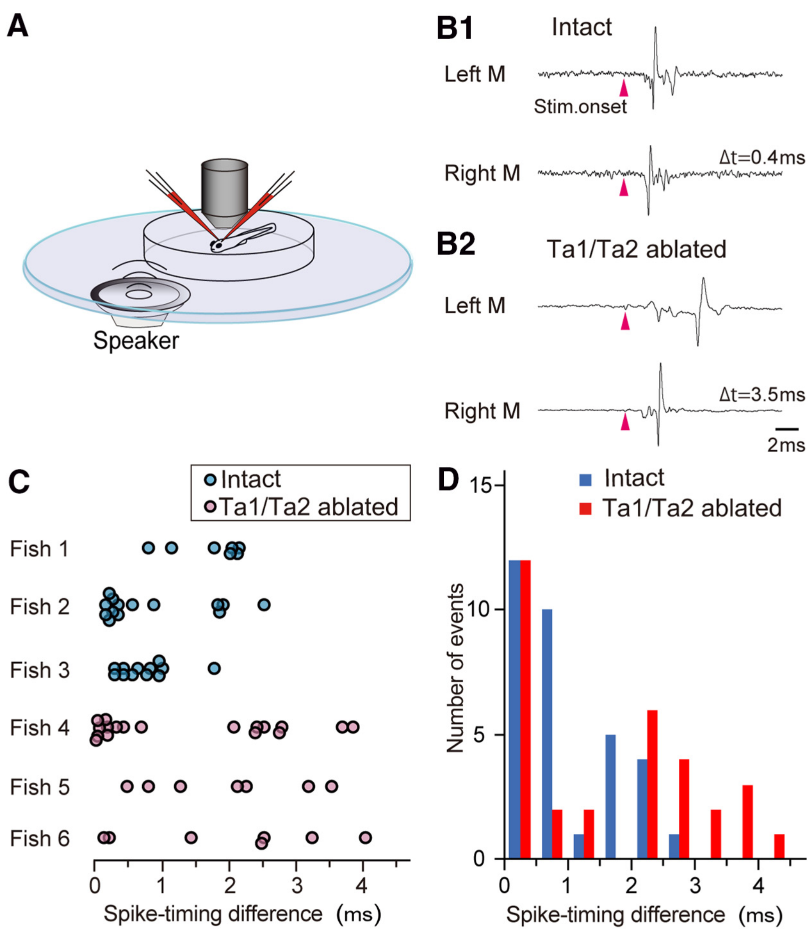

Figure 7. Loose-patch recordings from bilateral M cells fired by sound/vibration stimulus. ***A***, Schematic illustration of the apparatus to deliver a sound/vibration stimulus during electrophysiological recordings. ***B***, Examples of spike responses of bilateral M cells in an intact animal (***B1***) and in an animal in which Ta1/Ta2 neurons on both sides were ablated (***B2***). ***C***, Plots of the spike-timing differences of intact (blue) and Ta1/Ta2-ablated animals (red). ***D***, Accumulated data from ***C*** representing spike-timing differences between bilateral M cells.

performance in escape behaviors. We were especially interested in the following possibility: coactivations of two M cells during the effective period of the reciprocal inhibition (from 2 to tens of milliseconds after the first M cell spike) (Takahashi et al., 2002) would result in poorer escape performance because of disruptive effects of the second (trailing) M cell spike. It should be noted that, in intact animals, coactivation of the two M cells with a shorter time difference (<2 ms) did not obviously impair the animal's escape performance because inhibitory circuits mediated by CoLo neurons in the spinal cord (Satou et al., 2009) almost completely cancel the excitatory effects of the trailing M cell spike (for more details, see Discussion).

We examined the effects of unilateral ablation of Ta1 and Ta2. Figure 8*A*, *B* shows representative escape responses elicited by sound/vibration stimuli (as shown in Fig. 6*A2*) in a fish where Ta1 and Ta2 were ablated on the right side. In this configuration, reciprocal inhibition from the right M cell to the left M cell is greatly reduced, whereas that from the left M cell to the right M cell remains intact. Thus, this configuration has an internal control in the same animal. Our expectation was that escapes toward the left side would be affected, whereas escapes toward the right side would remain normal. We tested this idea by comparing the escape performance to one direction with that to the other direction.

In the experiments, sudden sound/vibration stimuli were applied to elicit escape behaviors. Then, the maximum turn angle (Fig. 8*A*,*B*, asterisks) was measured for each trial. As we expected, the maximum C bend angle of left turns (affected side) was often smaller than that of right turns (control side), as shown in a representative example (Fig. 8*C*). Figure 8*D* shows population data in the experiments of Ta1/Ta2 ablation on the right side. The maximum turn angles of left turns (pink) and right turns (blue) were plotted in a vertical column for each animal. For all the animals ($n = 6$ fish), the average (black horizontal line) of the left turns (affected side) was smaller than that of the right turns (control side) ($p = 0.031$, Wilcoxon signed-rank test). We then performed the experiments in which Ta1/Ta2 neurons on the left side were ablated. As expected, the average maximum turn angle of the right turns (affected side) was smaller than that of the left turns (control side) for all the examined animals (Fig. 8*E*; $n = 7$ fish) ($p = 0.016$, Wilcoxon signed-rank test). It should be noted that the average maximum turn angle to the control side in these experiments (132 ± 2.3 degrees, 54 trials from 13 animals) was not significantly different from the average maximum turn angle of intact fish (131 ± 1.4 degrees, 86 trial from 10 animals).

In Figure 8*F*, all the data from all the animals ($n = 13$ fish) were collected and shown as histograms. Turns toward the unaffected side are shown in blue (total trials, 54), whereas those toward the affected side are shown in red (total trials, 55). The distribution patterns of these two are clearly different ($p < 10^{-3}$, Mann–Whitney *U* test). For the turns to the unaffected (control) side, the peak of the distributions was ~125–130 degrees. By contrast, for the turns to the affected side, the peak was ~110 degrees. This value corresponded to the lowest observed values for the turns to the unaffected side (only two occurrences in total). For the affected side, turns with even smaller values of 95–105 degrees were observed. Turns with these values were not observed for the unaffected side.

Behavioral experiments in the animals in which Ta1/Ta2 neurons and one of the M cells are ablated: the role of reciprocal inhibition during escapes

The results thus far described revealed that the unilateral ablations of Ta1 and Ta2 neurons resulted in shallower turns toward the affected side on average. We favor the following scenario to account for the phenomena. The unilateral ablations of Ta1/Ta2 led to the unilateral reduction of the reciprocal inhibition, which resulted in frequent coactivation of the two M cells. Notably, delayed action potentials with a time difference exceeding ~2 ms after the first M cell spike only occurred in one of the M cells located on the contralateral side of the ablation. Under these conditions, escape performance was impaired to the affected side because of the contradictory excitatory effects of the delayed M cell spike on the opposite side of the escape turn.

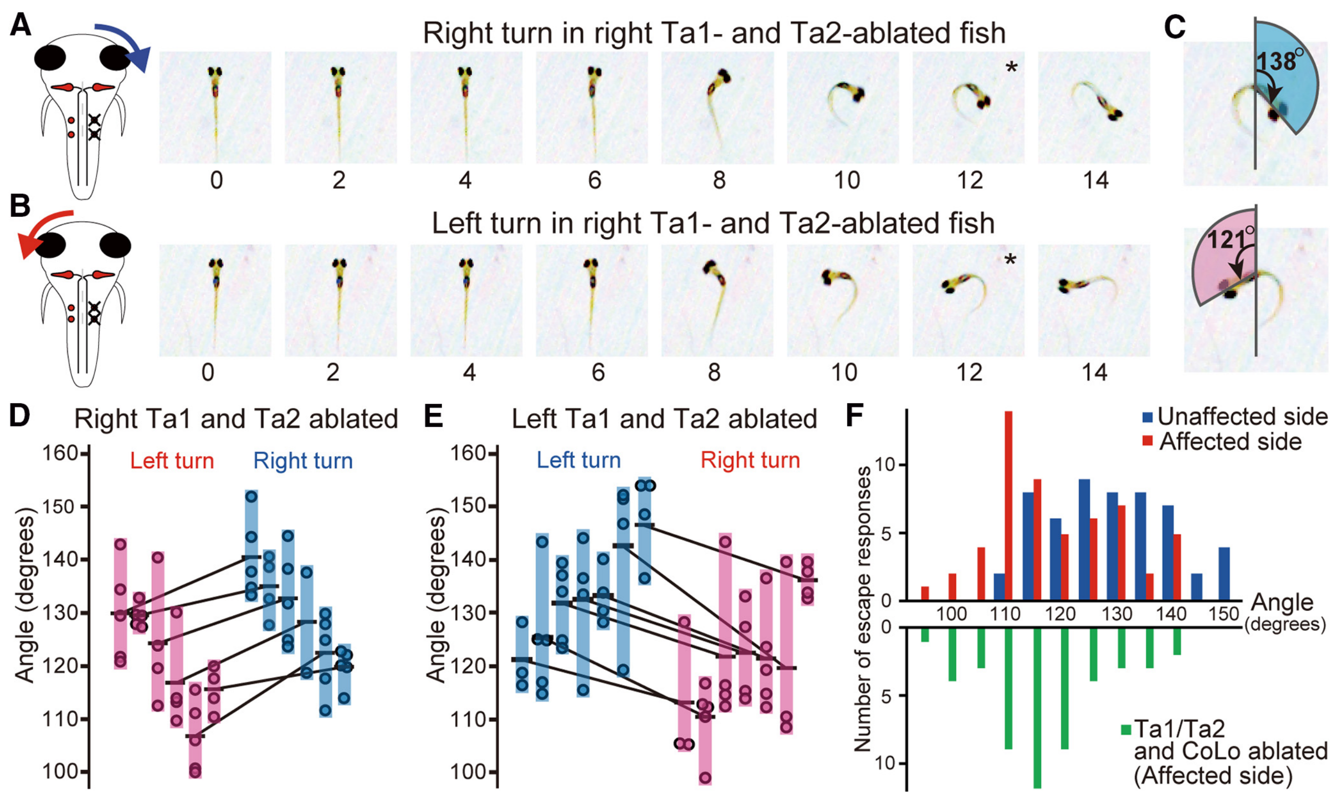

Figure 8. Behavioral experiments in the animals in which Ta1 and Ta2 neurons are ablated. Ta1 and Ta2 neurons were unilaterally ablated in the experiments. ***A***, ***B***, Examples of escape turns in an animal in which Ta1/Ta2 neurons on the right side were ablated. ***A***, Example of a right turn. ***B***, Example of a left turn. A sound/vibration stimulus was applied at the time point marked by "0." Images were collected at 1000 frames/s. Every other frame is shown (2 ms between frames). *Bend angle of the body is maximum at that frame. ***C***, Calculation of the maximum bend angles in the trials shown in ***A*** and ***B***. ***D***, Population data in the experiments of Ta1/Ta2 ablation located on the right side. The maximum bend angles of left turns (pink) and right turns (blue) are plotted in a vertical column for each animal. Black horizontal lines indicate the averages. For each animal, the average values of the left turn and the right turn are compared by connecting them with a thin line. ***E***, Population data in the experiments of Ta1/Ta2 ablation located on the left side. The maximum bend angles of left turns (blue) and right turns (pink) are plotted in a vertical column for each animal. ***F***, Upward bars represent histograms of the maximum bend angles collected from all the trials (54 turns to the unaffected side; 55 turns to the affected side) from all the animals ($n = 13$). Escapes turns toward the ablated side are categorized as "unaffected side" (blue), and those toward the opposite side are categorized as "affected side" (red). Downward bars (green) represent histograms of the maximum bend angles in the animals in which Ta1/Ta2 and CoLo neurons were unilaterally ablated. Escape turns to the affected side (contralateral side to the ablations) were analyzed (50 turns from 10 animals).

Although the above-described explanation can account for the phenomena, we cannot rule out the possibility that other factors may have a greater impact on these shallower escape bends. For example, CRNs are known to relay M-cell excitations to cranial muscles (i.e., jaw muscles) (Hackett and Faber, 1983a) and pectoral fin muscles (Auerbach and Bennett, 1969). Impairments of this relay functions by the Ta1/Ta2 ablations could affect escape performances. In addition, CRNs may have unidentified functions: these neurons may relay M cell excitations to other reticulospinal neurons (Neki et al., 2014). If they have such functions, impairments of these functions could affect escape performances. To show that the reduction of escape bend angles was primarily caused by increased coactivations of the two M cells, we performed the experiments in which unilateral ablations of Tal/Ta2 were further accompanied by the ablation of the M cell on the contralateral side. Because only one M cell was present, the direction of escapes was fixed: only toward the "affected side" in terms of Ta1/Ta2 ablations. However, delayed action potentials of the other M cell could not occur due to the absence of the cell. Therefore, if escape performance was not impaired in this situation, we could conclude that delayed action potentials of the M cell ought to be the primary cause of the impaired escapes seen in the animals of unilateral Ta1/Ta2 ablations. We tested whether this was the case or not.

Unlike the experiments described in the previous section (unilateral ablations of just Ta1/Ta2), the current experiments did not have an internal control: we needed to compare the escape angles in different animals. To exclude the possibility that differences in genetic background would affect results, we performed the experiments using offspring obtained from the same pair. Figure 9 shows the summary of the results. As described in the previous section, simple Ta1/Ta2 ablations led to the reductions of escape bends to the affected side (compare the data for blue and pink; 6 fish; it should be noted that the data in this figure are included in Fig. 8). In other animals where the contralateral M cell was ablated on top of the Ta1/Ta2 ablations, impaired escapes were not observed (data shown in green; 6 fish). The maximum bend angles for all the trials were >120 degrees. This is in sharp contrast to the data for the affected side shown in pink: for more than half of the trials, the maximum bend angles were <120 degrees ($p < 10^{-3}$, Mann–Whitney U test). These results strongly suggest that coactivation of the two M cells was the primary cause for the shallower escape angles shown in the animals with the unilateral ablations of Ta1/Ta2.

Behavioral experiments in partially restrained larvae combined with calcium imaging of the M cells: the role of reciprocal inhibition during escapes

We further sought direct evidence that coactivations of the M cells were primarily responsible for shallower escape bends in Ta1/Ta2-ablated larvae. Toward this end, we performed behavioral experiments in head-fixed larvae while simultaneously ob-

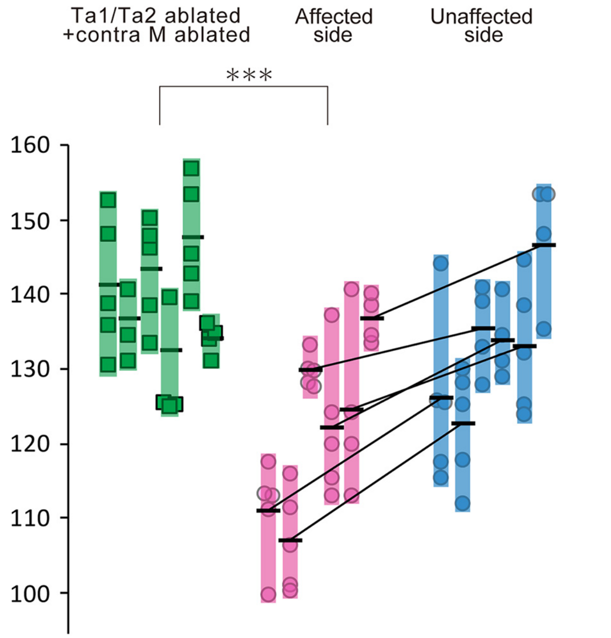

Figure 9. Behavioral experiments in the animals in which Ta1/Ta2 neurons and one of the M cells are ablated. In the experiments shown in green, unilateral ablations of Tal/Ta2 were accompanied by the ablation of the M cell on the contralateral side ($n = 3$ for left Ta1/Ta2 and right M-cell ablations; $n = 3$ for right Ta1/Ta2 and left M-cell ablations). The directions of the escapes were always contralateral to the remaining M cell. The maximum bend angles of the turns are plotted in a vertical column for each animal. Black horizontal lines indicate the averages. The experiments shown in blue and pink are the same as those shown in Figure 7 (unilateral ablations of only Ta1 and Ta2 neurons; $n = 3$ for right side ablations, $n = 3$ for left side ablations). Escapes turns toward the Ta1/Ta2-ablated side are categorized as "unaffected side" (blue), and those toward the opposite side are categorized as "affected side" (pink). ***$p < 0.001$ (Mann–Whitney U test).

serving M-cell activities with calcium imaging. The expectation was that shallower tail-flexion escapes were accompanied by coactivations of the M cells in Ta1/Ta2-ablated larvae.

Ta1 and Ta2 neurons were bilaterally ablated, and escapes were elicited in head-fixed larvae. Consistent with the calcium imaging experiment described in an earlier section (Fig. 6), the probability of bilateral M-cell activation was high (73.7%). As shown in Figure 10*A*, the amplitude of the escape bend was measured at the time frame of 8 ms after the onset of the movement (approximately corresponding to the time frame of the maximum bend in the case of escapes in unrestrained animals). As shown in the representative examples (Fig. 10*B*), escapes with shallower tail bends were occasionally observed when both of the M cells were activated. Figure 10*C* shows the results of each fish separately ($n = 3$). Figure 10*D* pools all the data from the 3 fish. The distribution patterns of these two are clearly different ($p < 10^{-3}$, Mann–Whitney U test) with very shallow bends (e.g., <20 degrees) only occurring upon M-cell coactivations.

The results of this experiment together with the experiment described in the previous section (Ta1/Ta2 ablation plus M-cell ablation) indicate that the bilateral activations of the M cells were the primary cause for the shallower escape angles shown in the Ta1/Ta2-ablated animals.

Behavioral experiments in the animals in which Ta1/Ta2 neurons and one side of the CoLo neurons are ablated

As a possible mechanism for accounting for the shallower C bend in the Ta1/Ta2-ablated animals upon coactivations of M cells, misactivation of CoLo neurons of the nonescape side upon the delayed arrivals of the second M cell spike would inhibit the motor outputs of the escape side (for more details, see Discussion). To examine whether misactivation of CoLo neurons contributed to this phenomenon, we performed behavioral experiments in which unilateral ablation of Tal/Ta2 was further accompanied by the ablation of the CoLo neurons on the same side. Maximum bend angles of the escapes toward the affected side were examined. The results are appended in Figure 8*F* as downward green bars. The distribution of the green bars is similar to that of the red bars (the maximum bend angles to the affected side without further ablation of the CoLo neurons). The mean values were 118 ± 1.4 degrees (green) and 121 ± 1.6 degrees (red). There was no significant difference between the two groups ($p = 0.219$, t test). Thus, additional ablation of CoLo neurons did not obviously affect the results. These results suggest that possible misactivation of CoLo neurons of the nonescape side did not significantly contribute to the shallower C bend in the Ta1/Ta2-ablated animals (for more details, see Discussion).

Discussion

In this study, we first identified two CRNs, Ta1 and Ta2, using the Tol-056 enhancer trap line. Taking advantage of the line, we showed the following: (1) Ta1 and Ta2 played a major role in producing reciprocal/recurrent inhibition in the M-cell network; (2) under the conditions of the weakened reciprocal inhibition (Ta1/Ta2 ablation), the occurrence probability of bilateral activation of the two M cells greatly increased; (3) the increase of the bilateral activation was attributed to those events in which the time difference of the two M cell spikes exceeded ~2 ms; and (4) with the increased occasions of bilateral activation of the two M cells upon Ta1/Ta2 ablation, escape performances were often impaired with C bend reduced. Collectively, these results show that bilateral activation of the M cells with the prolonged time differences results in poorer escape performance, thus indicating the importance of the reciprocal inhibition for an animal's behaviors.

Functional role of the reciprocal inhibition between the M cells in the hindbrain and its relationship with the crossed inhibition mediated by CoLo neurons in the spinal cord

In addition to the reciprocal inhibition between two M cells, the M-cell network has an important crossed inhibitory system in the spinal cord that is mediated by a special class of inhibitory neurons called CoLo (Satou et al., 2009). Because the CoLo-mediated inhibition is important when interpreting the phenotypes observed in this study, we discuss its role and its relationship with the reciprocal inhibition between the two M cells.

We first explain how the two inhibitory circuits work in intact animals (Fig. 11*A*,*B*). Figure 11*A* shows a typical escape with unilateral activation of the M cell. When the left M cell fires, reciprocal inhibition between the M cells suppresses the activation of the right M cell. Ta1 and Ta2 play a major role in this pathway. Figure 11*B* shows an escape with bilateral activation of the two M cells. This occasionally occurs in intact animals, as there is a gap in the reciprocal inhibition of M cells (~2 ms). In other words, the time difference between the two M spikes in an intact animal is within this narrow time window. Upon bilateral activation, CoLo-mediated inhibitions almost completely suppress the excitatory effects of the second (trailing) M spike on the left side of the body, resulting in an almost normal escape. This hyperfast inhibition is enabled by electrotonic transmission between M-CoLo synapses (Satou et al., 2009).

In Ta1/Ta2-ablated animals (Fig. 11*C*,*D*), reciprocal inhibition is significantly reduced. In this situation, the probability of

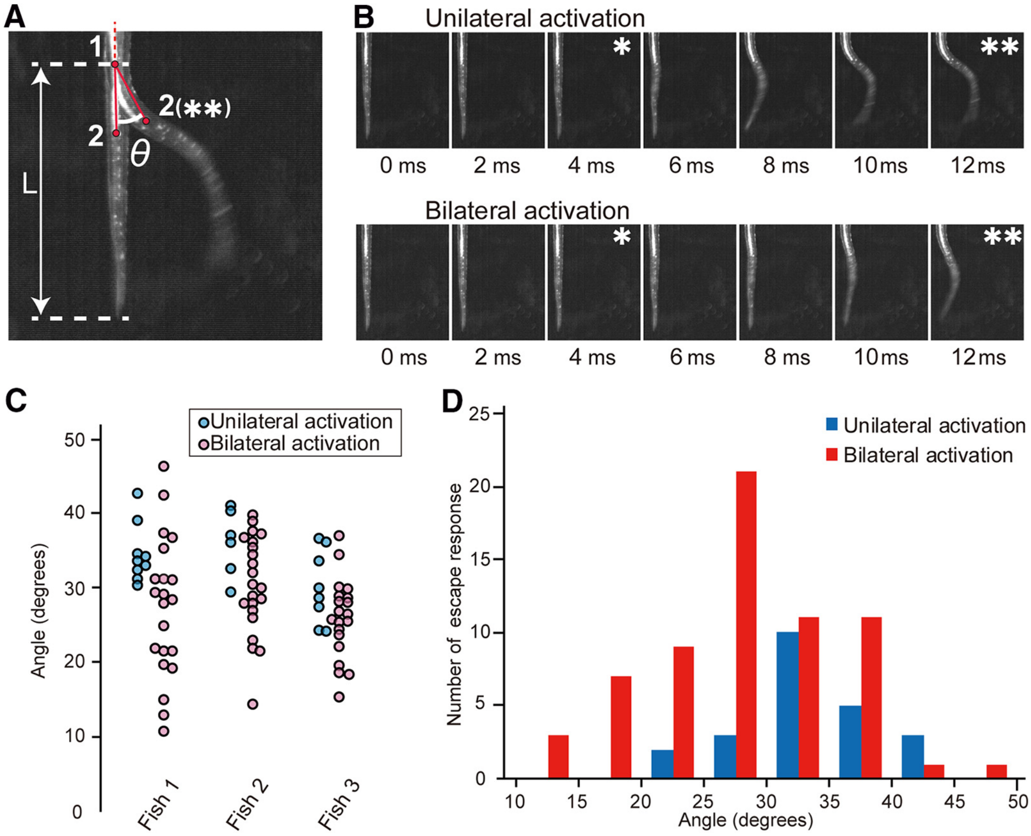

Figure 10. Behavioral experiments in partially restrained larvae combined with calcium imaging of the M cells. Ta1 and Ta2 neurons were bilaterally ablated in the experiments. Dextran-conjugated Cal-590 indicator was injected into the spinal cord of a larva of the Tol-056 line to label the M cells with the dye. The rostral part of the larva was embedded in agar while the tail part was kept free. The cutting position of the agar was set at three segments rostral to the cloaca. ***A***, The tail flexion angle was measured using the two body positions on the midline. Position 1 was set at the edge of the agar. Position 2 was set at a quarter length of the free-tail part (L). The line between the two positions at the time frame of 8 ms (**) after the onset of the movement was drawn. Then the angle between this line and the body line before the movement was determined (θ). ***B***, Examples of the escape response when only one of the M cells fired (top) and when both of the M cells fired (bottom). Numbers below panels indicate time after the onset of the sound/vibration stimulus. *Onset of flexion. **8 ms after the movement. ***C***, Plot of the flexion angle. For each animal ($n = 3$), the data on the occasions of unilateral M-cell activations and bilateral M-cell activations are separately plotted for comparison purposes. ***D***, Graph showing all the data pooled from all the animals.

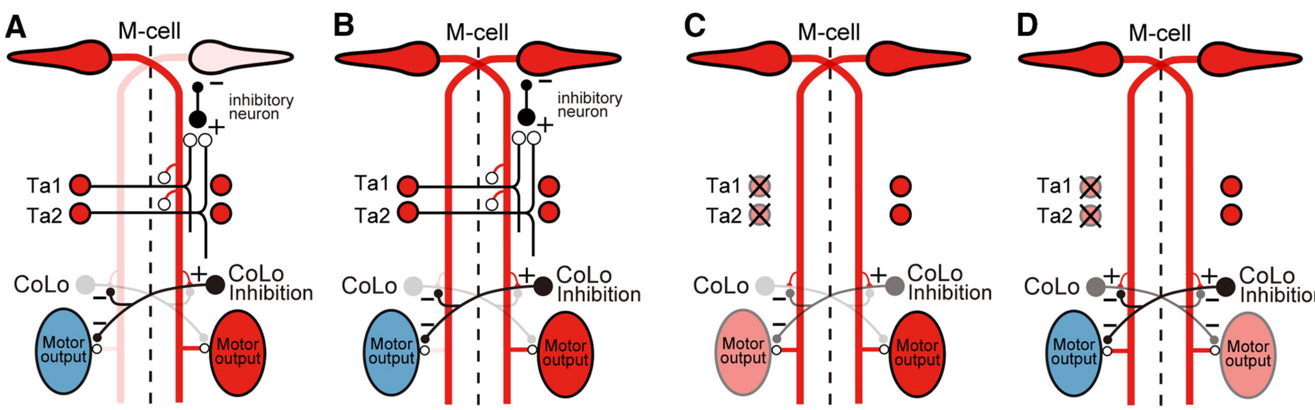

Figure 11. Schematic illustrations for the explanation of the motor activities with the reduced reciprocal inhibition. In all figures, dark red represents a fully active state, whereas blue represents an inactive state. ***A***, An intact animal with a unilateral activation of the M cell (left side). The action potential of the left M cell led to the activation of Ta1 and Ta2 neurons, which inhibited the right M cell. The inhibition makes the right M cell silent. The motor activity occurs only on the right side of the body. ***B***, An intact animal with bilateral activations of the two M cells with the time difference of the spikes being within a very short time window (~2 ms). Reciprocal inhibition between the M cells is not effective within this time range. This figure assumes that the left M cell is the first to fire. Despite the coactivation of the two M cells, the motor activity on the left side along the entire body is suppressed by the crossed inhibitions mediated by CoLo neurons, resulting in a normal escape toward the right (Satou et al., 2009). ***C***, A Ta1/Ta2-ablated animal with bilateral activation of the two M cells (the left one is the first to fire) with the time difference of the two spikes being beyond the time window of the reciprocal inhibition (~2 ms). In the spinal cord, the crossed inhibitions mediated by the right CoLo neurons suppress the motor activity on the left side. However, because of the larger time difference, the inhibition becomes weaker and cannot completely suppress a fraction of the excitatory components, resulting in some motor activity (pink oval). This contradictory motor activity has negative effects on the escape toward the right. ***D***, The same situation as in ***C***. In this figure, however, some of the left CoLo neurons are assumed to have recovered from the crossed CoLo inhibitions, and became active. The activated left CoLo neurons provide crossed inhibition to the right side, resulting in insufficient motor activity on the right side (pink oval).

bilateral M-cell activation is greatly increased (Fig. 6). This is attributed to the occurrences of bilateral activation with the second M cell spike falling in the effective period of the reciprocal inhibition (~>2 ms, Fig. 7). Even under such conditions, animals can still perform escapes, but their performances are impaired (Fig. 8). A likely scenario describing the observed shallower C bend is that some of the excitatory neurons (including motoneurons) on the left side are activated by the trailing (right) M cell spike due to a weakening of CoLo inhibition with the prolonged late arrival of the trailing M spike. This delayed activation of excitatory neurons and motoneurons induces weak motor outputs on the left side (Fig. 11*C*, pink oval). These outputs contradict the motor outputs on the right side (Fig. 11*C*, red oval). Another possible scenario is that some of the CoLo neurons on the left side are activated by the trailing (right) M cell after recovery from the contralateral (right) CoLo inhibition, and the activation of the left CoLo partially inhibits the contralateral (right side) motor outputs (Fig. 11*D*, pink oval). In either case, for Ta1/Ta2-ablated fish, the asymmetry between bilateral motor outputs is weakened and a reduced C bend is produced. The two scenarios shown in Figure 11*C*, *D* are not mutually exclusive: both may contribute to reducing the C bend angles. Our results from additional CoLo ablation experiments (Fig. 8*F*) suggest that any contribution of the latter possibility (Fig. 11*D*) is not high.

In the current study of very brief sound/vibration stimuli, time differences of the two M cell spikes were not long (<4 ms even in the Ta1/Ta2-ablated animals), resulting in slight reductions of the maximum bend angles. Depending on stimulation types, the time differences of the two M cell spikes, in the absence of reciprocal inhibition, could be much longer. In such cases, escape performances would be further impaired, as greater numbers of CoLo's targets, whose activities ought to be suppressed, get excited due to weakening inhibition.

In this study, we used the maximum bend angles of the initial turns as the measures for evaluating escape performances. A previous study showed that the maximum bend angle is an important factor for determining the ultimate escape directions — an escape behavior consists of an initial turn, a counter turn, and fast swimming (Eaton and Emberley, 1991). This supports the evaluation method used in this study.

Ta1 and Ta2 constitute major, but not all, components of CRNs

Electrophysiological studies have shown that Ta1 and Ta2 constitute major components of CRNs in their function of relaying reciprocal/recurrent inhibition: both types of inhibition are significantly reduced in Ta1/Ta2-ablated larvae (30%–40% of reduction; Figs. 4, 5). Yet, this also means that Ta1 and Ta2 cannot account for all of the functions of CRNs, suggesting the presence of other CRNs. The prime candidates for these CRNs are the T reticular neurons that are more caudally located than Ta1 and Ta2 (Fig. 2*C1*,*C2*). A previous anatomical study (Kimmel et al., 1985) showed that all the T reticular neurons have a similar morphology and are repeatedly present along the rostrocaudal axis at regular intervals. Thus, they are assumed to be composed as a serial duplication.

Recurrent inhibition of the M cell

In the current study, we did not observe successive firings of the same M cells in Ta1/Ta2-ablated animals despite the reduction of recurrent inhibition. This is somewhat unsurprising given that, upon a square current injection, the M cells tend to fire just once, even without recurrent inhibition, because of their intrinsic membrane properties (Watanabe et al., 2014, 2017). One important feature of recurrent as well as reciprocal inhibition is its long-lasting effects (tens of milliseconds; Fig. 5) (Takahashi et al., 2002). Recurrent inhibition may play important roles in preventing multiple firings of the M cell on a longer time scale (i.e., 30 ms).

Multiple organizations of commissural inhibitions in the brain and spinal cord

The present study, combined with our previous study (Satou et al., 2009), strongly suggests that two types of commissural inhibition operate to achieve full body bending during fish escape: reciprocal inhibition between a pair of M cells in the hindbrain and CoLo inhibition in the spinal cord. CoLo neurons play an important role during bilateral activation of the two M cells (Satou et al., 2009). In a very short time range (within ~2 ms), CoLo inhibition relayed by electrical coupling between the M cell and glycinergic CoLo neurons plays a pivotal role in preventing bilateral contraction of trunk muscles. Beyond this time range, the reciprocal inhibition between the bilateral M cells is recruited to prevent the second M cell firing. The suppressing effect of M cell reciprocal inhibition lasts over tens of milliseconds (Takahashi et al., 2002). In contrast, the present study suggests that CoLo-mediated inhibition in the spinal cord gradually decreases within the time range of several milliseconds. Thus, commissural inhibitions in the hindbrain and spinal cord are cooperating with partially overlapping, but different, time scales, and the combination of the two ensures asymmetric activities within a bilateral CNS. Eliminating either of them results in the inability to properly produce the asymmetric movement.

It should be noted that the organizations of the two types of commissural inhibitions differ. In the spinal cord, the inhibition is directly mediated by glycinergic commissural neurons (CoLo neurons). In contrast, the commissural inhibition in the hindbrain is mediated by commissural excitatory neurons (CRNs). These CRNs make synaptic connections onto local inhibitory neurons, which ultimately inhibit target neurons. The utilization of relay-type excitatory neurons may add versatility in neuronal circuits — CRNs are also involved in relaying excitations to cranial motoneurons — and may be a common design in a higher level of CNS. Interestingly, a critical role of excitatory commissural interneurons in the brain is suggested in the lateralized motor control of mammals, including humans. To achieve the lateralized activation of the motor cortex, the active motor cortex is thought to inhibit the contralateral corresponding cortex (Hübers et al., 2008), and the circuit is thought to be mediated by transcallosal excitatory neurons that make connections with local inhibitory interneurons innervating pyramidal cells in the cortex (Meyer et al., 1995; Reis et al., 2008). The assumed circuit framework resembles the reciprocal inhibition between the bilateral, command-like M cells; and in this sense, the reciprocal inhibitions in fish escape circuits may serve as a cellular model for the investigation of lateralized activation of the motor cortex in mammals.

References

Auerbach AA, Bennett MV (1969) Chemically mediated transmission at a giant fiber synapse in the central nervous system of a vertebrate. J Gen Physiol 53:183–210. CrossRef Medline

Beaulé V, Tremblay S, Théoret H (2012) Interhemispheric control of unilateral movement. Neural Plast 2012:627816. CrossRef Medline

Bellardita C, Kiehn O (2015) Phenotypic characterization of speed-associated gait changes in mice reveals modular organization of locomotor networks. Curr Biol 25:1426–1436. CrossRef Medline

Bhatt DH, Otto SJ, Depoister B, Fetcho JR (2004) Cyclic AMP-induced repair of zebrafish spinal circuits. Science 305:254–258. CrossRef Medline
Burgess HA, Granato M (2007) Sensorimotor gating in larval zebrafish. J Neurosci 27:4984–4994. CrossRef Medline
Diamond J (1971) The Mauthner cell. Fish Physiol 5:265–346. CrossRef
Dunn TW, Mu Y, Narayan S, Randlett O, Naumann EA, Yang CT, Schier AF, Freeman J, Engert F, Ahrens MB (2016) Brain-wide mapping of neural activity controlling zebrafish exploratory locomotion. Elife 5:1–29. CrossRef Medline
Eaton RC, Emberley DS (1991) How stimulus direction determines the trajectory of the Mauthner-initiated escape response in a teleost fish. J Exp Biol 161:469–487. Medline
Eaton RC, Lavender WA, Wieland CM (1981) Identification of Mauthern-initiated response patterns in goldfish: evidence for simultaneous cinematography and electrophysiology. J Comp Physiol 144:521–531. CrossRef
Faber DS, Korn H (1978) Electrophysiology of the Mauthner cell: basic properties, synaptic mechanisms, and associated networks. In: Neurobiology of the Mauthner cell, pp 47–131. New York: Raven.
Faber DS, Fetcho JR, Korn H (1989) Neuronal networks underlying the escape response in goldfish. Ann N Y Acad Sci 563:11–33. CrossRef Medline
Fetcho JR, Faber DS (1988) Identification of motoneurons and interneurons in the spinal network for escapes initiated by the Mauthner cell in goldfish. J Neurosci 8:4192–4213. CrossRef Medline
Furukawa T, Furshpan EJ (1963) Two inhibitory mechanisms in the neurons of goldfish. J Neurophysiol 26:140–176. CrossRef Medline
Grillner S, Matsushima T (1991) The neural network underlying locomotion in lamprey-synaptic and cellular mechanisms. Neuron 7:1–15. CrossRef Medline
Hackett JT, Faber DS (1983a) Mauthner axon networks mediating supraspinal components of the startle response in the goldfish. Neuroscience 8:317–331. CrossRef Medline
Hackett JT, Faber DS (1983b) Relay neurons mediate collateral inhibition of the goldfish Mauthner cell. Brain Res 264:302–306. CrossRef Medline
Hackett JT, Cochran SL, Greenfield LJ Jr (1989) Quantal transmission at Mauthner axon target synapses in the goldfish brainstem. Neuroscience 32:49–64. CrossRef Medline
Holland LZ, Carvalho JE, Escriva H, Laudet V, Schubert M, Shimeld SM, Yu JK (2013) Evolution of bilaterian central nervous systems: a single origin? Evodevo 4:27. CrossRef Medline
Hübers A, Orekhov Y, Ziemann U (2008) Interhemispheric motor inhibition: its role in controlling electromyographic mirror activity. Eur J Neurosci 28:364–371. CrossRef Medline
Kiehn O (2016) Decoding the organization of spinal circuits that control locomotion. Nat Rev Neurosci 17:224–238. CrossRef Medline
Kimmel CB, Metcalfe WK, Schabtach E (1985) T reticular interneurons: a class of serially repeating cells in the zebrafish hindbrain. J Comp Neurol 233:365–376. CrossRef Medline
Kimura Y, Okamura Y, Higashijima S (2006) alx, a zebrafish homolog of Chx10, marks ipsilateral descending excitatory interneurons that participate in the regulation of spinal locomotor circuits. J Neurosci 26:5684–5697. CrossRef Medline
Kimura Y, Satou C, Fujioka S, Shoji W, Umeda K, Ishizuka T, Yawo H, Higashijima S (2013) Hindbrain V2a neurons in the excitation of spinal locomotor circuits during zebrafish swimming. Curr Biol 23:843–849. CrossRef Medline
Kohashi T, Oda Y (2008) Initiation of Mauthner- or non-Mauthner-mediated fast escape evoked by different modes of sensory input. J Neurosci 28:10641–10653. CrossRef Medline
Kohashi T, Nakata N, Oda Y (2012) Effective sensory modality activating an escape triggering neuron switches during early development in zebrafish. J Neurosci 32:5810–5820. CrossRef Medline
Korn H, Faber DS (2005) The Mauthner cell half a century later: a neurobiological model for decision-making? Neuron 47:13–28. CrossRef Medline
Koyama M, Pujala A (2018) Mutual inhibition of lateral inhibition: a network motif for an elementary computation in the brain. Curr Opin Neurobiol 49:69–74. CrossRef Medline
Koyama M, Kinkhabwala A, Satou C, Higashijima S, Fetcho J (2011) Mapping a sensory-motor network onto a structural and functional ground plan in the hindbrain. Proc Natl Acad Sci U S A 108:1170–1175. CrossRef Medline
Meyer BU, Röricht S, Gräfin von Einsiedel H, Kruggel F, Weindl A (1995) Inhibitory and excitatory interhemispheric transfers between motor cortical areas in normal humans and patients with abnormalities of the corpus callosum. Brain 118:429–440. CrossRef Medline
Moult PR, Cottrell GA, Li WC (2013) Fast silencing reveals a lost role for reciprocal inhibition in locomotion. Neuron 77:129–140. CrossRef Medline
Neki D, Nakayama H, Fujii T, Matsui-Furusho H, Oda Y (2014) Functional motifs composed of morphologically homologous neurons repeated in the hindbrain segments. J Neurosci 34:3291–3302. CrossRef Medline
O'Malley DM, Kao YH, Fetcho JR (1996) Imaging the functional organization of zebrafish hindbrain segments during escape behaviors. Neuron 17:1145–1155. CrossRef Medline
Orger MB, Kampff AR, Severi KE, Bollmann JH, Engert F (2008) Control of visually guided behavior by distinct populations of spinal projection neurons. Nat Neurosci 11:327–333. CrossRef Medline
Palmer LM, Schulz JM, Murphy SC, Ledergerber D, Murayama M, Larkum ME (2012) The cellular basis of GABAB-mediated interhemispheric inhibition. Science 335:989–993. CrossRef Medline
Reis J, Swayne OB, Vandermeeren Y, Camus M, Dimyan MA, Harris-Love M, Perez MA, Ragert P, Rothwell JC, Cohen LG (2008) Contribution of transcranial magnetic stimulation to the understanding of cortical mechanisms involved in motor control. J Physiol 586:325–351. CrossRef Medline
Roberts A, Conte D, Hull M, Merrison-Hort R, al Azad AK, Buhl E, Borisyuk R, Soffe SR (2014) Can simple rules control development of a pioneer vertebrate neuronal network generating behavior? J Neurosci 34:608–621. CrossRef Medline
Satou C, Kimura Y, Kohashi T, Horikawa K, Takeda H, Oda Y, Higashijima S (2009) Functional role of a specialized class of spinal commissural inhibitory neurons during fast escapes in zebrafish. J Neurosci 29:6780–6793. CrossRef Medline
Takahashi M, Narushima M, Oda Y (2002) In vivo imaging of functional inhibitory networks on the Mauthner cell of larval zebrafish. J Neurosci 22:3929–3938. CrossRef Medline
Takahashi M, Inoue M, Tanimoto M, Kohashi T, Oda Y (2017) Short-term desensitization of fast escape behavior associated with suppression of Mauthner cell activity in larval zebrafish. Neurosci Res 121:29–36. CrossRef Medline
Talpalar AE, Bouvier J, Borgius L, Fortin G, Pierani A, Kiehn O (2013) Dual-mode operation of neuronal networks involved in left-right alternation. Nature 500:85–88. CrossRef Medline
Tanimoto M, Ota Y, Horikawa K, Oda Y (2009) Auditory input to CNS is acquired coincidentally with development of inner ear after formation of functional afferent pathway in zebrafish. J Neurosci 29:2762–2767. CrossRef Medline
Watanabe T, Shimazaki T, Mishiro A, Suzuki T, Hirata H, Tanimoto M, Oda Y (2014) Coexpression of auxiliary Kv 2 subunits with Kv1.1 channels is required for developmental acquisition of unique firing properties of zebrafish Mauthner cells. J Neurophysiol 111:1153–1164. CrossRef Medline
Watanabe T, Shimazaki T, Oda Y (2017) Coordinated expression of two types of low-threshold K^+ channels establishes unique single spiking of Mauthner cells among segmentally homologous neurons in the zebrafish hindbrain. eNeuro 4:ENEURO.0249-17.2017. Medline
Yasargil GM, Diamond J (1968) Startle-response in teleost fish: an elementary circuit for neural discrimination. Nature 220:241–243. CrossRef Medline
Yasargil GM, Sandri C (1990) Topography and ultrastructure of commissural interneurons that may establish reciprocal inhibitory connections of the Mauthner axons in the spinal cord of the tench, *Tinca tinca L.* J Neurocytol 19:111–126. CrossRef Medline
Zhou W, Saint-Amant L, Hirata H, Cui WW, Sprague SM, Kuwada JY (2006) Nonsense mutations in the dihydropyridine receptor β1 gene, CACNB1, paralyze zebrafish relaxed mutants. Cell Calcium 39:227–236. CrossRef Medline
Zottoli SJ (1977) Correlation of the startle reflex and Mauthner cell auditory responses in unrestrained goldfish. J Exp Biol 66:243–254. Medline